Lawrence M. White, MD
Jae K. Kim, MD, PhD
Mitesh Mehta, MD
Naeem Merchant, MD
Mark E. Schweitzer, MD
William B. Morrison, MD
Carol R. Hutchison, MD
Allan E. Gross, MD

Index terms:
Hip, abnormalities, 44.20, 44.454
Hip, MR, 44.121411, 44.121413, 44.121415, 44.121416, 44.12143
Hip, prostheses, 44.454
Magnetic resonance (MR), pulse sequences, 44.121411, 44.121413, 44.121415, 44.121416

Radiology 2000; 215:254–262

Abbreviation:
THA = total hip arthroplasty

[1] From the Dept of Medical Imaging, Mount Sinai Hospital and the University Health Network, University of Toronto, 600 University Ave, Toronto, Ontario, Canada M5G 1X5 (L.M.W., J.K.K., M.M., N.M.); Dept of Orthopedic Surgery, Mount Sinai Hospital, Toronto (C.R.H., A.E.G.); and Dept of Radiology, Thomas Jefferson University Hospital, Philadelphia, Pa (M.E.S., W.B.M.). From the 1998 RSNA scientific assembly. Received Feb 12, 1999; revision requested Mar 30; final revision received Jul 28; accepted Aug 30. Supported in part by RSNA Research and Education Foundation and a grant from Berlex, Canada. **Address reprint requests to** L.M.W. (e-mail: *lwhite@mtsinai.on.ca*).

Author contributions:
Guarantors of integrity of entire study, L.M.W., J.K.K., M.M.; study concepts and design, L.M.W., J.K.K., M.M., M.E.S.; definition of intellectual content, L.M.W., J.K.K., M.M.; literature research, L.M.W., J.K.K., M.M.; clinical studies, L.M.W., M.M., W.B.M.; experimental studies, L.M.W., J.K.K.; data acquisition, L.M.W., J.K.K., M.M., W.B.M., N.M.; data analysis, L.M.W., J.K.K., M.M., N.M., A.E.G., C.R.H.; statistical analysis, L.M.W.; manuscript preparation, L.M.W., J.K.K.; manuscript editing, L.M.W., J.K.K., M.E.S.; manuscript review, L.M.W., J.K.K., C.R.H., A.E.G., M.E.S.

Complications of Total Hip Arthroplasty: MR Imaging—Initial Experience[1]

PURPOSE: To investigate the use of standard magnetic resonance (MR) imaging sequences with simple parameter modifications for the detection and characterization of total hip arthroplasty (THA) complications.

MATERIALS AND METHODS: An initial phantom study was performed with cobalt-chrome and titanium prostheses to establish the imaging parameters for a subsequent clinical study. In the clinical study, coronal and transverse MR imaging of 14 THA prostheses was performed before and after intravenous contrast material administration in 12 patients who were being considered for revision arthroplasty. The images were reviewed for evidence of juxtaarticular or periprosthetic abnormalities, patterns of contrast enhancement, and quality of periprosthetic tissue depiction.

RESULTS: Phantom study results showed improved periprosthetic tissue depiction with use of thin sections, increased frequency-encoding gradient strength, and fast spin-echo sequences. The clinical study results demonstrated periprosthetic abnormalities in 11 cases: mechanical loosening in two cases (including one case with an associated periprosthetic fracture); granulomatosis, eight; and infection, one. In 100% of cases, tissue depiction around the femoral component was judged to be of ''diagnostic quality.'' Tissue depiction around the acetabular component was of diagnostic quality in five (36%) cases. In all seven surgically confirmed cases, a correct diagnosis was made preoperatively with MR imaging.

CONCLUSION: By using simple modifications to standard MR imaging sequences, diagnostic-quality MR imaging of THA complications can be performed, particularly around the femoral prosthetic stem.

During the past 30 years, total hip arthroplasty (THA) has become a common, routine treatment for patients with hip arthrosis. Approximately 800,000 THA procedures are performed throughout the world each year (1). Of these, more than 120,000 THA procedures are performed annually in the United States (2). The local complications of THA procedures are well recognized and include heterotopic bone formation, mechanical aseptic loosening, prosthetic or periprosthetic fracture, dislocation, superficial and deep infections, and foreign-body granulomatosis (ie, osteolysis). Such complications are a common source of patient morbidity and often necessitate revision arthroplastic surgery.

The appropriate examination of a symptomatic patient who has undergone THA includes diagnostic imaging evaluation. This can involve radiography (3), nuclear medicine studies with bone and gallium scanning (4), joint aspiration (4,5), and arthrography (6,7). Cross-sectional imaging, however, typically is not used because of imaging artifacts caused by metal hip prostheses. These imaging artifacts include beam-hardening artifacts at computed tomography (CT) and metal susceptibility artifacts at magnetic resonance (MR) imaging.

Investigators have described the use of simple strategies to decrease the MR imaging artifacts caused by a variety of metal orthopedic devices used throughout the body (8–13). These strategies have included selective orientation of the frequency-encoding direction along the long axis of the device (8,12,13), reducing the voxel size (9,13), increasing the readout gradient strength (9,12), using fast spin-echo imaging (8–12), and using lower static magnetic field strengths.

Despite the prevalence of THA procedures, however, few MR studies have focused on

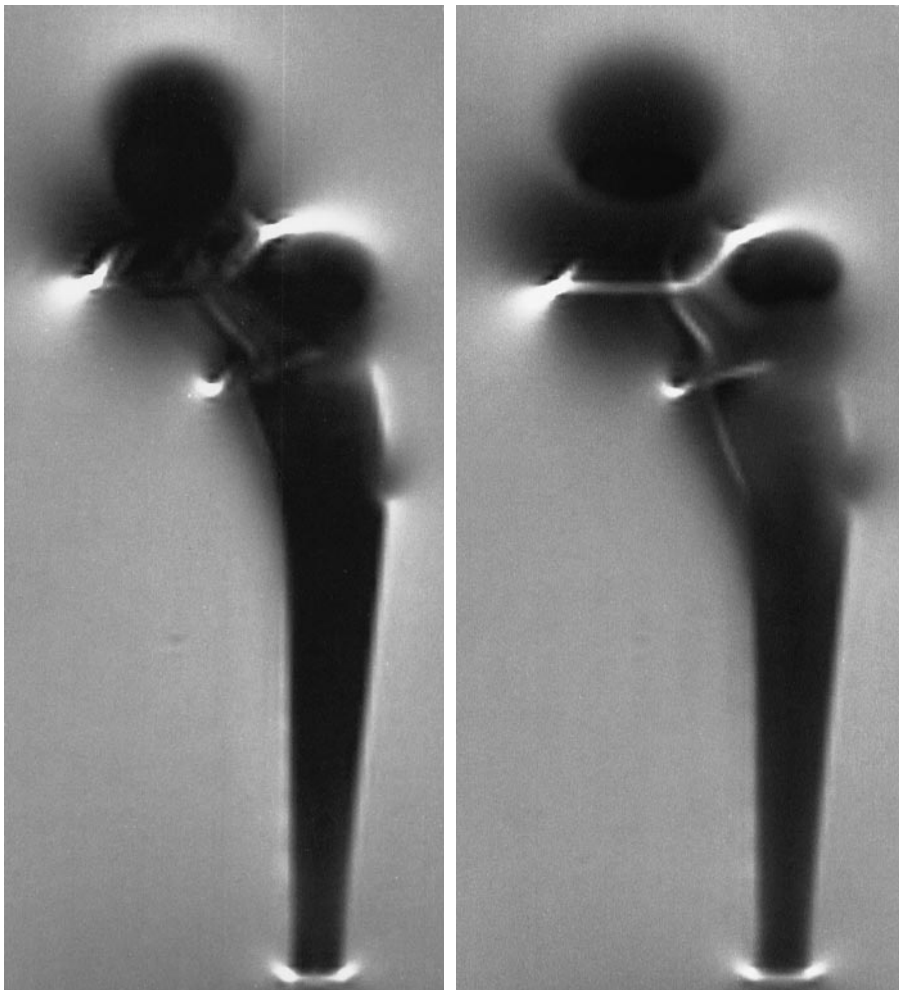

a. b.

Figure 1. Artifact caused by section-thickness variation. **(a, b)** Coronal MR images (2,000/15) through the center of a titanium femoral prosthesis in a gelatin phantom, with section thicknesses of **(a)** 5 and **(b)** 10 mm. The 5-mm section thickness was noted empirically to enable better periprosthetic visualization without a noticeable effect on the signal-to-noise ratio and thus was chosen for use in the clinical study.

imaging around the metal orthopedic hip prostheses (10,12,14). Tormanen et al (12) performed an in vitro investigation that focused on optimizing standard MR sequences for imaging around metal orthopedic hip implants. Potter et al (10) performed an in vivo investigation that focused on the use of MR angiography for the detection of deep venous thrombosis and use of MR imaging for the detection of hip dislocation in patients who had undergone THA previously.

Lemmens et al (14) performed an earlier clinical MR imaging study of THA prostheses with a 0.5-T magnet. The results of this investigation indicated good depiction of loosening around the distal part of the femoral component of a THA prosthesis. Elsewhere, however, poorer depiction of periprosthetic soft tissue was noted.

Higher magnetic field strengths, however, are associated with proportionately larger metal artifacts. This has contributed to the continuing and prevailing notion that MR imaging is not appropriate for the assessment of possible THA complications. To our knowledge, no clinical study to date has focused on MR imaging of the numerous periprosthetic complications of metal hip implants at 1.5 T, nor have there been further studies performed with lower magnetic field strengths.

In this study, we performed an initial clinical investigation aimed at assessing the feasibility of using standard MR imaging sequences at 1.5-T magnetic field strength and with simple imaging parameter modifications for the assessment of various complications of primary THA.

MATERIALS AND METHODS

Imaging System

All MR imaging examinations were performed with a clinical 1.5-T MR imaging system (Signa 5.4; GE Medical Systems, Milwaukee, Wis) by using a phased-array torso coil (Medical Advances, Milwaukee, Wis) with a maximum gradient strength of 10 mT/m.

Initial Gelatin Phantom Study

An initial gelatin phantom study was performed by using cobalt-chrome and titanium alloy femoral prostheses to help establish the section thickness and frequency-encoding gradient strength criteria for the patient study. A brief summary of the effects of magnetic static field inhomogeneities on MR images and simple methods to reduce these effects is provided in the Appendix.

Both types of prostheses were placed into separate plastic tubs filled with 2.6% commercially available gelatin. The prostheses were positioned longitudinally at the isocenter of the magnet. MR imaging was performed by using a coronal intermediate-weighted fast spin-echo sequence. The frequency-encoding direction was set along the longitudinal axis of the prosthesis. Coronal sections were obtained by using the following imaging parameters: 2,000/13–25 (repetition time msec/echo time msec), echo train length of four, 30-cm field of view, 256 × 256 matrix, and one signal acquired. The section thicknesses varied between 5, 10, and 20 mm. The readout bandwidths (commensurate with frequency-encoding gradient strength for the same field of view) varied between 8, 16, and 32 kHz. In addition, standard coronal intermediate-weighted spin-echo imaging with similar parameters was performed to qualitatively assess the differences between spin-echo and fast spin-echo imaging.

Patient Study

All patients were referred to our institution for orthopedic consultation and consideration for revision arthroplastic surgery. Fourteen metal hip implants in 12 patients (seven women, five men; mean age, 65 years; age range, 41–83 years) were studied. The mean time between the primary THA procedure and imaging was 15 years (range, 6 months to 30 years). All patients presented with complaints of pain and/or had abnormalities at radiography. The symptomatic complaints included local hip-groin pain in seven patients, hip and thigh pain in two patients,

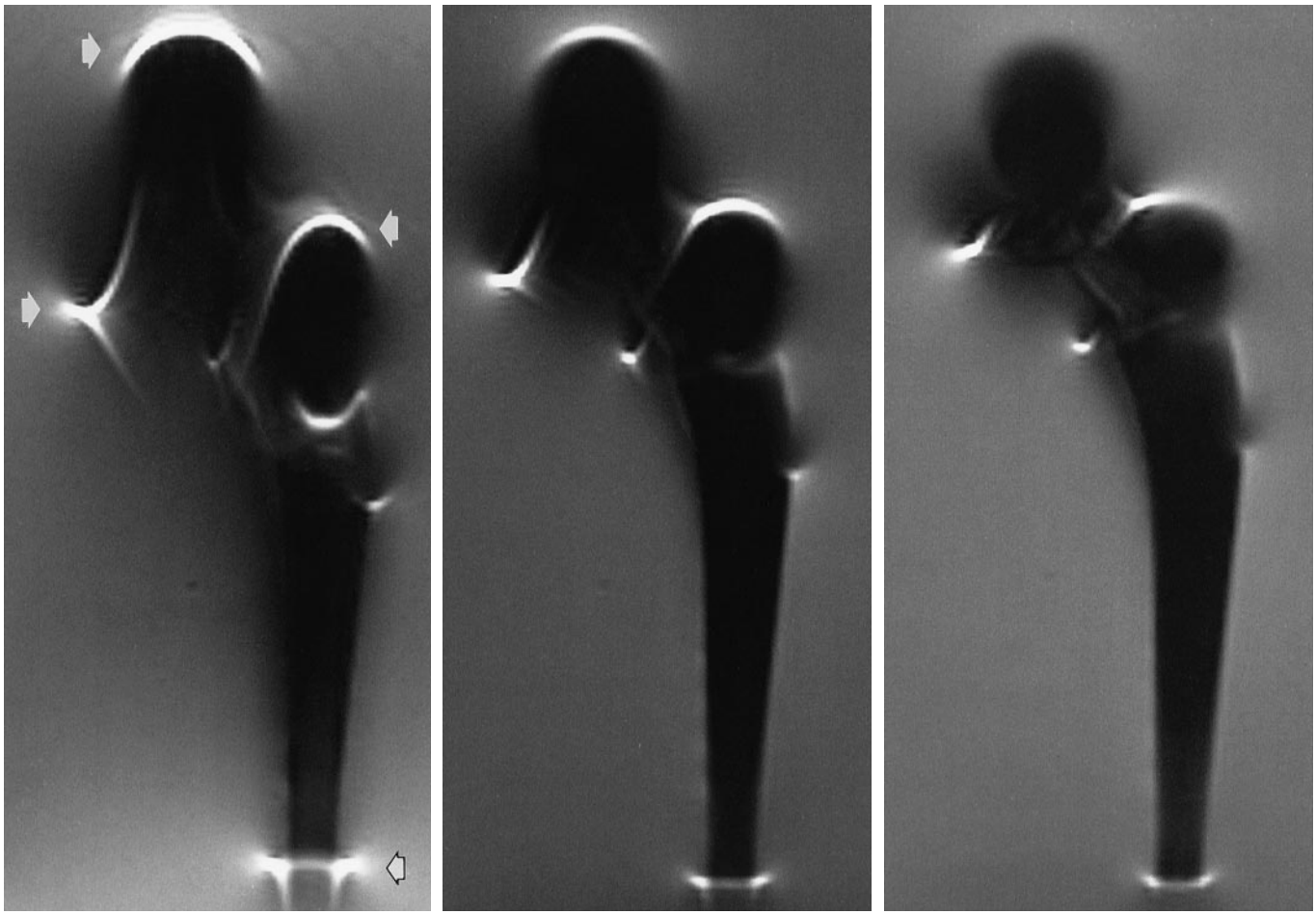

a. b. c.

Figure 2. Artifact variation with frequency-encoding gradient strength. **(a–c)** Coronal MR images (2,000/15) of a titanium femoral prosthesis obtained by using **(a)** 8-, **(b)** 16-, and **(c)** 32-kHz bandwidths for the corresponding field of view show the effect of increasing the frequency-encoding gradient strength on misregistration artifact (arrows in **a**). The change in this parameter resulted in the greatest visible artifact reduction. In the transition from a 16-kHz to 32-kHz readout bandwidth, the linear misregistration of the edge of the signal void was halved.

and isolated thigh pain and radiating pain from the hip to the knee, respectively, in one patient each. One patient was asymptomatic but had a focal area of periprosthetic hyperlucency in the proximal femur. In the two patients who had undergone bilateral arthroplasty, both hip implants were imaged. Thirteen of the hip prostheses were composed of a cobalt-chrome alloy, and one was composed of stainless steel.

Four THA prostheses were cemented, seven were not cemented, and three were hybrid devices with cemented acetabular components and noncemented femoral prostheses. Cement fixation, however, was not expected to have a major effect on imaging (15).

MR Imaging Parameters

Transverse T2-weighted images were acquired by using a fast spin-echo sequence. The imaging parameters were 4,500–5,500/100, echo train length of 16, 5-mm section thickness with no intersection gap, 22–30-cm field of view, 32-kHz readout bandwidth, 256 × 192 matrix, and three signals acquired.

Coronal fast inversion-recovery (ie, fast multiplanar inversion-recovery) images were obtained with a relatively long echo time to provide T2 weighting. The imaging parameters were 5,000/40/150 (inversion time msec), echo train length of eight, 5-mm section thickness with no intersection gap, 22-cm field of view, 256 × 192 matrix, and two signals acquired.

Transverse and coronal T1-weighted images were acquired with a T1-weighted fast spin-echo sequence. The imaging parameters were 450–600/10–15, echo train length of four, section thicknesses of 10 mm for transverse images and 5 mm for coronal images with no intersection gap, 22–30-cm field of view, 32-kHz readout bandwidth, 256 × 256 matrix, and two signals acquired.

T1-weighted sequences were used before and after the intravenous administration of 2.0 mL/kg gadopentetate dimeglumine (Magnevist; Berlex Laboratories, Wayne, NJ) into the antecubital fossa. To avoid problems caused by the inhomogeneity of spectral fat suppression in the vicinity of the metal prostheses, no fat suppression was used at postcontrast T1-weighted imaging.

Image Evaluation

The MR images were reviewed independently by two radiologists (L.M.W., N.M.) who were blinded to the radiographic findings and clinical symptoms. The images were assessed for evidence of juxtaarticular or periprosthetic fluid collections, periprosthetic osseous defects, peripros-

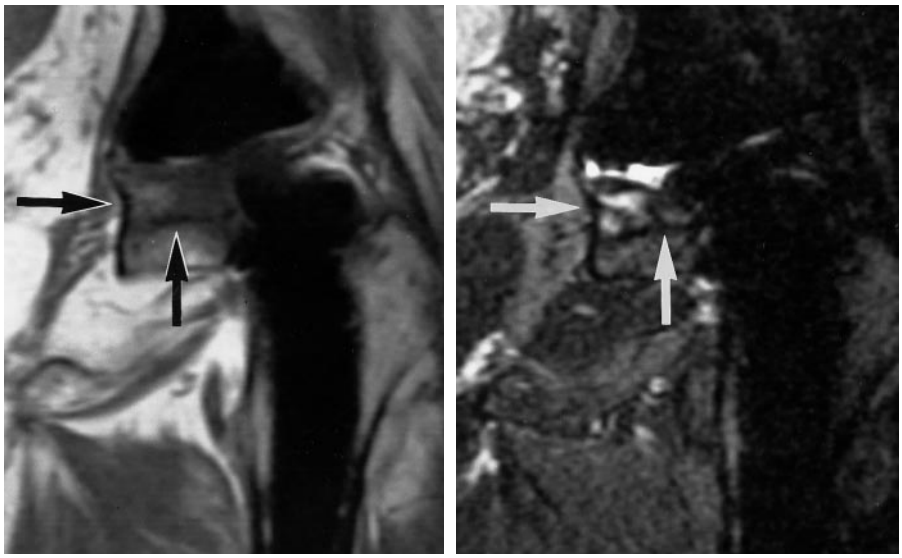

a. b.

Figure 3. Foreign-body granulomatosis. **(a)** Coronal, T1-weighted fast spin-echo image (500/10; echo train length, four) shows a low-signal-intensity mass (arrows) within the posterior column of the acetabular wall adjacent to the inferomedial aspect of the acetabular prosthesis. **(b)** Corresponding coronal, T2-weighted fast multiplanar inversion-recovery image (5,000/40/150, echo train length of eight) shows a heterogeneous, predominantly low- to intermediate-signal-intensity mass (arrows).

thetic soft-tissue masses, and patterns of periprosthetic enhancement.

In cases in which revision arthroplasty was subsequently performed, the surgical pathologic findings of periprosthetic tissue specimens were correlated with the prior MR imaging findings. In addition, each observer made a qualitative assessment of the bone and soft-tissue resolution surrounding the prosthetic components. The periprosthetic structures assessed included juxtaprosthetic marrow and cortical bone, as well as the normal soft-tissue structures surrounding the acetabulum and proximal femur, including the sciatic nerve and obturator, iliopsoas, and adductor musculature. Periprosthetic image quality was considered to be poor or nondiagnostic when there was no depiction of periprosthetic structures, good when there was diagnostic but suboptimal resolution of periprosthetic bone and soft tissue, or excellent when there was clear depiction of periprosthetic structures.

Interobserver variability in the assessment of periprosthetic image quality around the acetabular and femoral components was recorded, and a weighted κ statistic was calculated (16).

RESULTS

Initial Gelatin Phantom Study

The results of the initial gelatin phantom study demonstrated a typical signal void profile on the coronal sections of both the cobalt-chrome and titanium prostheses (Fig 1). The head of these prostheses has an essentially spherical geometry. The signal void around the head of the prosthesis developed in a clover leaf–like pattern, mainly because of section thickness variation around a spherical metal source (17) but also because of misregistration artifact (Fig 2). This was particularly apparent with the cobalt-chrome prostheses. Around the femoral stem, the signal void was linear and followed the longitudinal axis of the prosthesis. At the tip of the stem, depending on the direction of misregistration, a small focal region of signal void was seen. As expected, artifacts were less marked surrounding the titanium prosthesis (9,18). As a result, the frequency-encoding gradient was oriented parallel to the long axis of the femoral prostheses during our clinical study to decrease the degree of artifact along the bone prosthetic interface of the femoral prosthetic stem (8,12,13).

In varying the section thicknesses between 5 and 10 mm, the 5-mm section thickness was noted empirically to enable better visualization of the periprosthetic gelatin without a noticeable effect on the signal-to-noise ratio. In addition, increasing the frequency-encoding gradient strength produced a large, visible artifact reduction. As expected (13), with the transition from a 16-kHz to 32-kHz readout bandwidth, the linear misregistration of the edge of the signal void was halved.

With our MR imaging system, as with most clinical MR imaging systems, a 32-kHz readout bandwidth is the highest currently available bandwidth option on the operator console. A 32-kHz readout bandwidth was therefore chosen for our clinical study (9,12).

As expected, a mild improvement in the appearance but not in the size of the signal voids was noted with the use of fast spin-echo imaging versus spin-echo imaging (11). Only fast spin-echo imaging sequences were therefore used in our study.

Patient Study

By using the imaging techniques described, periprosthetic abnormalities were detected at MR imaging of 11 of the 14 metal hip implants (in 11 patients) assessed by both observers. Three arthroplastic prostheses demonstrated no focal periprosthetic abnormalities at MR imaging.

Seven of the 11 patients with periprosthetic abnormalities at MR imaging subsequently underwent THA revision. In each of these cases, the surgical and pathologic findings correctly correlated with the prior MR imaging findings. Two cases showed evidence of mechanical loosening, one of which had an associated periprosthetic fracture. Four cases demonstrated foreign-body granulomatosis. One case of infection also was demonstrated. The remaining four patients with periprosthetic abnormalities at MR imaging, who had not undergone surgery at the time this article was written, all had MR imaging findings that were consistent with foreign-body granulomatosis. Three of these patients are currently awaiting THA revision surgery. Revision surgery has been deferred for the last patient owing to a superimposed medical condition.

In all eight suspected or proved cases of foreign-body granulomatosis, a focal periprosthetic intraosseous mass with low T1 signal intensity and heterogeneous, predominately low to intermediate T2 signal intensity was seen (Figs 3, 4). With the intravenous administration of contrast material, all cases of suspected foreign-body granulomatosis demonstrated peripheral enhancement and some irregular internal enhancement. Five of the cases involved granulomatosis situated around both the femoral and acetabular components. One case involved the acetabular component only, and two involved the femoral component only. Of the four

cases of granulomatosis in which the patient underwent surgery (all proved to be positive), two involved both the femoral and the acetabular periprosthetic tissue, and two involved only the periprosthetic aspect of the femoral component.

In both proved cases of mechanical loosening, low-signal-intensity fluid collections parallel to the femoral prosthetic stem were observed (Fig 5). In one of these cases, associated femoral prosthetic penetration of the adjacent bone cortex indicated a periprosthetic fracture that was subsequently confirmed during surgery (Fig 6).

In the proved case of infection, a peripherally enhancing juxtaarticular fluid collection communicating with the underlying arthroplastic implant was consistent with infection and juxtaarticular abscess formation (Fig 7).

In terms of image evaluation, there was excellent (26/28 [93%] interpretations) interobserver agreement in the qualitative assessment of periprosthetic image resolution, with a weighted κ value of 0.90. Depiction of the periprosthetic bone and soft tissue surrounding the femoral prosthesis component on the acquired MR images was considered by the first reviewer to be excellent in six of 14 cases. The second reviewer judged seven cases as having excellent periprosthetic depiction. Depiction was considered by both reviewers to be good in all the remaining cases. No acquired MR image was judged to have poor or nondiagnostic depiction of tissue around the femoral prosthesis component. Thus, the images of tissue surrounding all the femoral prosthesis components were of diagnostic quality in 100% of cases.

Depiction of the acetabular periprosthetic structures was judged to be excellent in two of 14 cases by the first reviewer and in one case by the second reviewer. Depiction was deemed good in three cases and four cases, respectively, by the two reviewers. Both reviewers judged the depiction of periacetabular structures to be poor in nine cases. Thus, depiction of the acetabular periprosthetic structures was considered by both reviewers to be of diagnostic quality in five (36%) of 14 cases.

The depiction of periprosthetic structures in the one case with a stainless steel prosthesis was judged by both reviewers to be good surrounding the femoral prosthesis and poor surrounding the acetabular component. No substantial differences in periprosthetic imaging artifacts between the cemented and noncemented prosthetic components were noted.

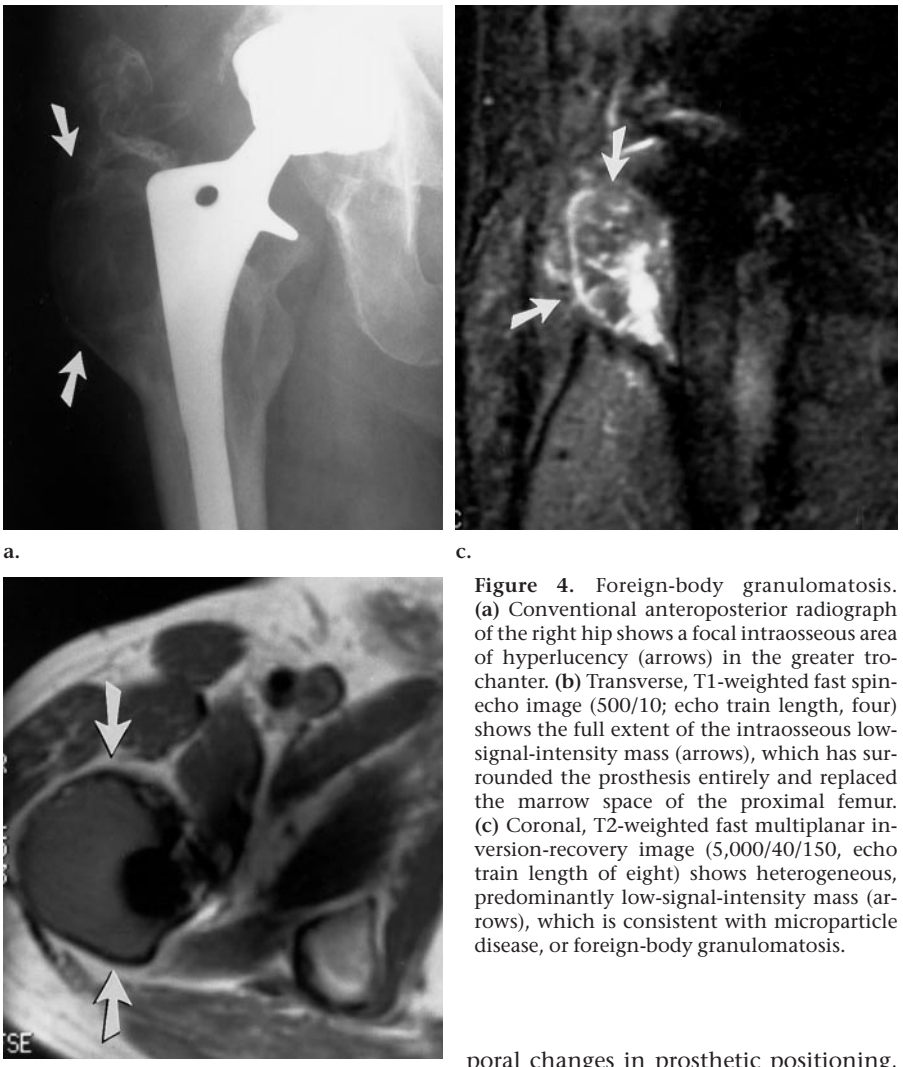

a. c.

b.

Figure 4. Foreign-body granulomatosis. **(a)** Conventional anteroposterior radiograph of the right hip shows a focal intraosseous area of hyperlucency (arrows) in the greater trochanter. **(b)** Transverse, T1-weighted fast spin-echo image (500/10; echo train length, four) shows the full extent of the intraosseous low-signal-intensity mass (arrows), which has surrounded the prosthesis entirely and replaced the marrow space of the proximal femur. **(c)** Coronal, T2-weighted fast multiplanar inversion-recovery image (5,000/40/150, echo train length of eight) shows heterogeneous, predominantly low-signal-intensity mass (arrows), which is consistent with microparticle disease, or foreign-body granulomatosis.

DISCUSSION

MR imaging has not been typically used for the diagnostic assessment of THA complications, probably because of the prevailing belief that metal-induced artifact obscures the desired detail. In this initial clinical investigation, however, the study results showed that common THA complications, especially those involving tissues around the femoral stem, can be diagnosed by using MR imaging with relatively simple imaging modifications (described in the Materials and Methods section and Appendix).

Mechanical loosening is usually diagnosed radiographically on the basis of periprosthetic areas of radiolucency, temporal changes in prosthetic positioning, and the filling of areas of periprosthetic hyperlucency with radiographic contrast material at joint arthrography. In this study, the two cases of mechanical loosening (both surgically proved) manifested on the preoperative images as nonenhancing fluid collections with low T1 signal intensity and high T2 signal intensity surrounding the femoral stem (Fig 5).

Foreign-body granulomatosis, or microparticle disease, is a process of local foreign-body reactions to various substrates of arthroplasty, including poly-methylmethacrylate, metal, and polyethylene; this condition results in periprosthetic bone loss. On radiographs, foreign-body granulomatosis typically manifests as lobulated regions of periprosthetic osteolysis. In this study, the cases of suspected foreign-body granulomatosis manifested as focal periprosthetic intraosseous masses with low T1 signal intensity and heterogeneous, predominately low to intermediate T2 signal intensity. With the intravenous administration of contrast material,

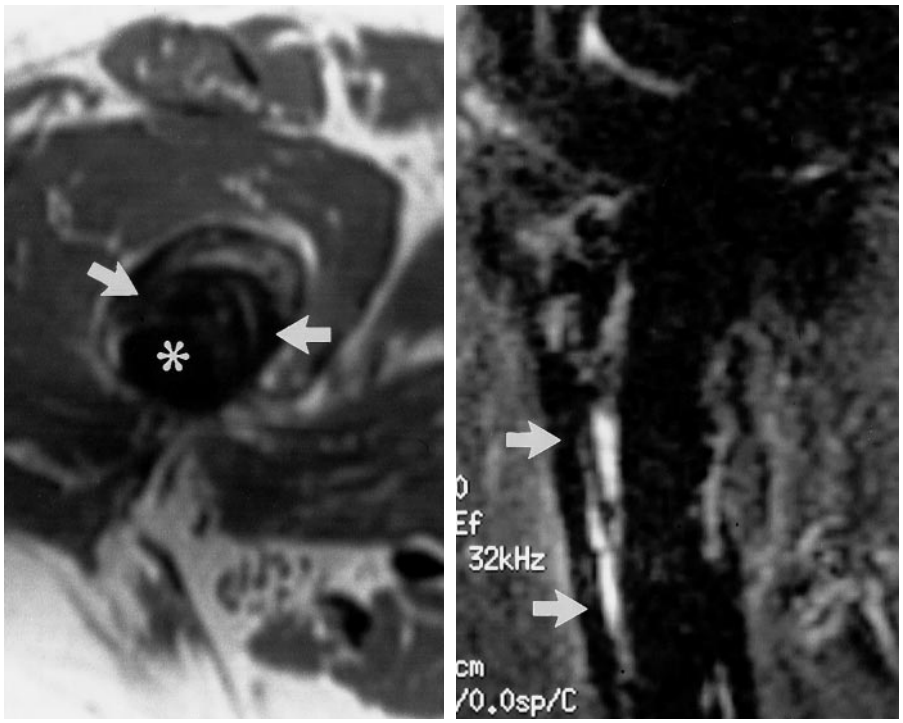

a. b.

Figure 5. Mechanical loosening. **(a)** Transverse, T1-weighted fast spin-echo image (500/10; echo train length, four) through the proximal femur shows a nonspecific area of low signal intensity (arrows) surrounding the femoral prosthetic stem (asterisk). **(b)** Coronal, T2-weighted fast multiplanar inversion-recovery image (5,000/40/150, echo train length of eight) shows an area of high signal intensity (arrows) paralleling the lateral aspect of the femoral stem; this finding is consistent with mechanical loosening.

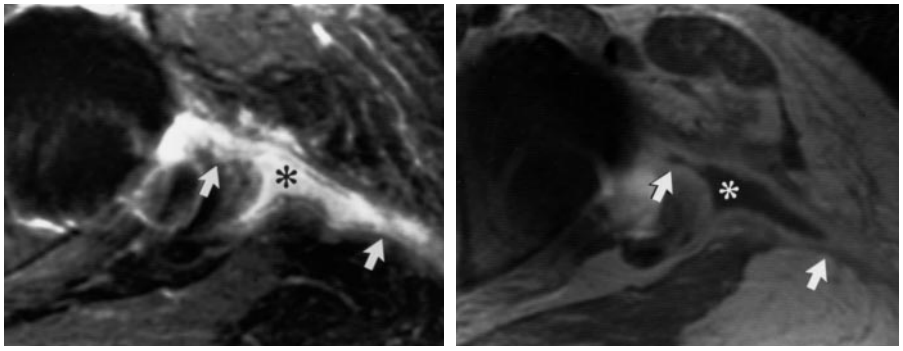

a. b.

Figure 7. Infection. **(a)** Transverse, T2-weighted fast multiplanar inversion-recovery image (5,000/40/150, echo train length of eight) shows an irregular area of high signal intensity (asterisk) along the soft tissues of the lateral region of the thigh. **(b)** On the corresponding T1-weighted fast spin-echo image (500/10; echo train length, four) obtained after the intravenous administration of gadopentetate dimeglumine, the central area of low signal intensity (asterisk) and peripheral rim enhancement of the mass are suggestive of an abscess collection. Sinus tracts (arrows in **a** and **b**) can be seen extending down to the THA prosthetic articulation and peripherally into the subcutaneous soft tissues.

foreign-body granulomatosis demonstrated peripheral enhancement and some irregular internal enhancement.

MR imaging has been shown to be highly sensitive and specific for the detection of osseous fractures (19–21). In the single case of periprosthetic fracture in this study, we observed cortical penetration of the proximal femur by the stem of the femoral prosthesis in the setting of

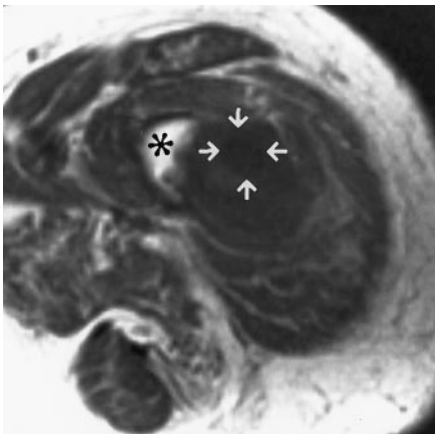

Figure 6. Transverse, T1-weighted fast spin-echo image (500/10; echo train length, four) shows a periprosthetic fracture of the proximal femur. Prosthetic penetration is seen through the cortex of the proximal femur, with the femoral prosthetic stem (arrows) extending anterolaterally into the soft tissues of the thigh. Normal bone marrow fat (asterisk) is seen medially within the residual portion of the femoral diaphysis.

underlying mechanical loosening (Fig 6). On the basis of the conventional radiographic findings, the patient acquired this fracture during the interval between initial clinical consultation and MR imaging. It is plausible that, with appropriate MR imaging, other types of fractures in addition to occult longitudinal periprosthetic fractures may be detected.

Infection is a relatively uncommon THA complication that is seen with less than 1% of all THA procedures performed (22). Radiographs in the setting of infection are often nonspecific, and the diagnostic evaluation for possible infection can include nuclear medicine imaging and/or joint aspiration. In the single case in this study, an irregular, peripherally enhancing fluid collection with low signal intensity at T1-weighted imaging and high signal intensity at T2-weighted imaging was demonstrated, and this high or low signal intensity communicated with the underlying prosthetic hip joint (Fig 7). Although all infections do not result in periarticular abscess or fluid collections, the presence of juxtaosseous fluid at MR imaging has been recognized as an important sign in the diagnosis of osteomyelitis (23–25). The specificity of the finding of periprosthetic fluid collections in the setting of pain following THA and the features that distinguish juxtaarticular abscess collections from fluid secondary to mechanical loosening are not yet known.

In this investigation, there was diagnos-

tic-quality depiction of the periprosthetic structures surrounding the femoral prostheses in 100% of cases according to the two observers. Reduced (36%) diagnostic depiction of the periprosthetic soft tissue and bone surrounding the acetabular components was noted. This latter result is reasonable, considering the complicated section thickness and orientation variation that occurs in the proximity of a structure with spherical geometry (17) and the complex influence of the metallic acetabular component.

The potential clinical use of MR imaging in the investigation of suspected THA complications was highlighted in three cases in which the MR imaging findings directly affected the subsequent clinical management. In one case, infection was diagnosed at MR imaging 6 months after the initial joint replacement. Clinical management was altered in this case, with joint aspiration, resection arthroplasty, and long-term antibiotic therapy initiated before revision arthroplastic surgery.

In the second case, the patient's radiographic findings suggested possible foreign-body granuloma formation within the proximal femur, but the MR images showed the fatty bone marrow to have normal signal intensity without a focal periprosthetic abnormality; these findings were suggestive of stress shielding. On the basis of the MR imaging findings in this patient, the initial plans for revision surgery were deferred.

In the third case, the MR images showed a large periprosthetic abnormality that was consistent with foreign-body granuloma involving the entire proximal femur (Fig 4). The preoperative surgical plan, which was initially based on the radiographic findings (Fig 4a), was altered. MR imaging delineated the size and extent of granuloma formation and the lack of residual bone stock within the proximal femur (Fig 4b, 4c). The initial treatment plans were changed from local curettage and impaction bone grafting to resection and allograft reconstruction of the proximal femur. MR imaging, therefore, aided in specifying the type and amount of bone grafting required for successful revision surgery; these factors may be particularly critical for surgical planning at centers that do not have an on-site bone bank.

One limitation of our study was the relatively small number of THA prostheses imaged; this was mainly because of our patient selection criterion. Only those patients who were being considered for revision surgery on the basis of radiographic and/or clinical abnormalities were selected. This criterion, however, allowed us to assess the imaging of advanced stages of disease and THA complications, which is ideal for an initial assessment of MR imaging of THA complications. Eventually, the capability of MR imaging to help assess the early changes of disease and THA complications will need to be investigated. It should be noted, however, that a large number of cases is not necessarily required to demonstrate a technique's ability to depict periprosthetic soft tissue and bone regions in the setting of THA.

Another limitation of our study was the fact that the three patients who did not have focal periprosthetic abnormalities at MR imaging did not undergo revision surgery. Thus, the negative findings in the study could not be confirmed. In addition, although MR imaging had a clinical effect in some of the cases described, no testing of the accuracy of the technique was performed as a component of this initial investigation. Thus, although MR imaging appears to be promising, the true clinical value of the technique in the setting of suspected THA complication has yet to be assessed.

In this initial investigation, we did not perform a direct comparison between MR imaging findings and radiographic findings. Although comparison of the relative sensitivity, specificity, and accuracy of MR imaging versus those of radiography in patients with suspected complications of THA may be an important future investigation, such a comparison was not attempted in this investigation. The purpose of this initial study was to assess the feasibility of using MR imaging, with simple modifications in technique, in the examination of patients with possible complications of primary THA.

Although it is clear that diagnostic-quality MR imaging around the femoral component can be performed, the difficulty in imaging around the acetabular component is a problem intrinsic to the geometry of the acetabular component and its effect on two-dimensional MR imaging. This remains a difficult problem to address efficiently.

Decreasing the primary magnetic field strength might be beneficial to MR imaging around metal hip implants. This would commensurately reduce geometric distortion artifact with the same frequency-encoding gradient strengths. The use of lower primary magnetic field strength should be considered, particularly with regard to its effect of reduced signal-to-noise resolution.

Using alternative MR imaging sequences or adaptations of those currently used may result in further minimization of metal artifacts. For instance, the use of three-dimensional techniques will help to reduce the voxel volume and eliminate the section thickness variation caused by static field distortions. These sequences, however, tend to be time-consuming. In addition, a two-dimensional, view-angle tilting adaptation, as described by Cho et al (26), may be implemented as a means of eliminating misregistration.

In conclusion, the use of MR imaging in examining patients with possible THA-related complications is an underinvestigated clinical area. The results of this study of 14 THA prostheses in symptomatic patients demonstrate that practical and consistent diagnostic-quality 1.5-T MR imaging of THA complications can be performed, especially around the femoral stem.

APPENDIX

MR Imaging Artifacts Associated with Metal Implants

The major MR imaging artifacts associated with metal implants are well known. These artifacts include geometric distortion of signal intensity in the frequency-encoding direction (also known as misregistration), section thickness variation due to altered excitation profiles in two-dimensional imaging, increased signal intensity loss due to diffusion effects from the paramagnetic implant, and substantially increased dephasing at gradient-echo imaging.

Misregistration in the frequency-encoding direction is well described and creates characteristic signal intensity variations, depending on the implant's shape and orientation (8,9,12,13,27). There is no misregistration in the phase-encoding direction because phase encoding performed with variable amplitudes is immune to misregistration.

Section thickness variation is a result of altered excitation profiles in a distorted primary magnetic field (9). In the presence of a mildly distorted primary magnetic field, an excited section takes on a warped appearance, as it follows isomagnetic lines within the imaging volume. In the presence of a ferromagnetic material—for example, a metal sphere—section thickness variation increases markedly and the profile of the section takes on a complex structure (17). Much of the signal void proximal to a spherical metal object is related to section thickness variation (17).

Diffusion-related signal intensity loss increases in the proximity of a metal implant. In spin-echo imaging, a refocusing pulse recovers the transverse signal intensity loss

caused by static influences such as primary magnetic field inhomogeneities and bulk susceptibility differences. Transverse signal intensity that is not recoverable with a refocusing pulse contributes to T2 relaxation. In the presence of very large magnetic field gradients, such as those imposed by a metal hip implant in its vicinity, randomly moving water molecules undergo increased spin dephasing that is not completely recoverable with a refocusing pulse. Therefore, near a metal implant, a long echo time, such as that in T2-weighted spin-echo imaging, causes increased signal intensity loss from random microscopic processes such as diffusion.

Unlike in spin-echo imaging, in gradient-echo imaging of metal implants there is no refocusing pulse and, thus, there is additional intravoxel dephasing (T2*) that creates marked signal voids. Although decreasing the voxel size (28) or shortening the echo time (29) can improve gradient-echo imaging to some degree, the extent of intravoxel dephasing with this sequence usually precludes its regular use in the evaluation of tissue around metal implants.

If spectral fat saturation is used during an MR imaging sequence, static field or applied radio-frequency inhomogeneities can cause nonuniform signal intensities (30).

Other MR imaging artifacts, such as those related to static field (4) or applied radio-frequency (31) eddy currents, exist. These, however, are relatively nonsubstantial in magnitude.

MR Imaging Metal Artifact Reduction Techniques

Simple modifications to imaging parameters can be made to reduce the MR imaging artifacts caused by metal implants. First, misregistration artifact is proportional to static field inhomogeneity and inversely proportional to applied frequency-encoding gradient strength. Therefore, increasing the frequency-encoding gradient strength decreases the misregistration artifact proportionately (12,32).

Second, selective orientation of the frequency- and phase-encoding gradients improves the resolution of tissues surrounding metal implants by changing the misregistration artifact direction (8,12,13). In addition, the degree of such a resultant misregistration signal void is smallest with metal implants that are oriented longitudinally in the static magnetic field (8,9,12,13,27).

Third, to our knowledge, the effect of variable section thickness has been largely ignored in previously published literature. With the femoral stem placed longitudinally in the primary magnetic field, minimal effects on section curvature and thickness in the transverse or coronal orientation would be expected because of the symmetric geometry of the stem (33). In the region of the prosthesis head, however, which is roughly spherical in geometry, extreme variation in section thickness can occur (17). Although increases or decreases in the selected section thickness may aid in visualization, the section thickness variation can be completely controlled only by using three-dimensional acquisition with phase encoding of the section-select direction. This option, however, is not always practical because of examination time constraints.

Fourth, fast spin-echo imaging techniques can produce a modest increase in MR signal intensity near metal implants owing to several complex reasons. Fast spin-echo imaging refocuses spins at a faster interval than does conventional spin-echo imaging and thus causes a small increase in signal intensity by reducing diffusion-related signal intensity loss. This effect increases with smaller interecho spacing (8). Furthermore, fast spin-echo sequences are robust to malrotations of signal. Malrotation of signal is a potential problem with spin-echo multiecho sequences, wherein malrotated signal interferes with the primary signal pathway and thus creates artifacts; this effect is markedly reduced with crusher gradients around each 180° pulse. The fast spin-echo k-space pathway, however, is special in that it causes most malrotated signal to run in phase with the primary signal pathway; no crusher gradients are required (34). Because fast spin-echo sequences use rather than eliminate malrotated signal, there is a modest increase in signal intensity relative to that with multiecho spin-echo sequences per effective echo time. Accordingly, fast spin-echo sequences can use 180° refocusing pulses that are slightly more spatially thick than the 90° excitation pulse, to result in better refocusing of excited signal without concern for increased regions of malrotation.

It should be noted that, contrary to common misconception, fast spin-echo imaging does not reduce signal voids created as a result of misregistration artifacts by reducing misregistration artifact, but rather it reduces these voids by increasing the signal intensity inherent in the described mechanisms.

Fifth, reducing the voxel size increases the spatial definition of implant-induced signal void and thus reduces the apparent size of the void (9). A simple technique to reduce the voxel size without increasing the examination time is to increase the number of pixels in the frequency-encoding direction (9). Furthermore, smaller voxels help to reduce diffusion-related signal intensity loss.

Sixth, the signal intensity variation associated with spectral fat saturation in a nonuniform magnetic field may be reduced by using a fast multiplanar inversion-recovery sequence, which is an effective fat saturation technique that is less vulnerable to magnetic field variation (30).

References

1. Herberts PG, Stromberg CN, Malchau H. Revision hip surgery: the challenge. In: Galante JO, Rosenberg AG, Callaghan JJ, eds. Total hip revision surgery: Bristol-Myers Squibb/Zimmer Orthopaedic Symposium series. New York, NY: Raven, 1995; 1–15.
2. NIH consensus conference. Total hip arthroplasty. JAMA 1995; 273:1950–1956.
3. Manaster BJ. Total hip arthroplasty: radiographic evaluation. RadioGraphics 1996; 16:645–660.
4. Kraemer WJ, Soplys R, Waddell JP, Morton J. Bone scan, gallium scan and hip aspiration in the diagnosis of infected total hip arthroplasty. J Arthroplasty 1993; 8:611–615.
5. Roberts P, Walters AJ, McMinn DJ. Diagnosing infection in hip replacement: the use of fine needle aspiration and radiometric culture. J Bone Joint Surg Br 1992; 74:265–269.
6. Maus TP, Berquist TH, Bender CE, Rand JA. Arthrographic study of painful total hip arthroplasty: refined criteria. Radiology 1987; 162:721–727.
7. Cheung A, Lachiewicz PF, Renner JB. The role of aspiration and contrast-enhanced arthrography in evaluating the uncemented hip arthroplasty. AJR Am J Roentgenol 1997; 168:1305–1309.
8. Eustace S, Jara H, Goldberg R, et al. A comparison of conventional spin-echo and turbo spin-echo imaging of soft tissues adjacent to orthopedic hardware. AJR Am J Roentgenol 1998; 170:455–458.
9. Petersilge CA, Lewin JS, Duerk JL, Yoo JU, Ghaneyem AJ. Optimizing imaging parameters for MR evaluation of the spine with titanium pedicle screws. AJR Am J Roentgenol 1996; 166:1213–1218.
10. Potter HG, Montgomery KD, Padgett DE, Salvati EA, Helfet DL. Magnetic resonance imaging of the pelvis: new orthopaedic applications. Clin Orthop 1995; 319:223–231.
11. Tartaglino LM, Flanders AE, Vinitski S, Friedman DP. Metallic artifacts on MR images of the postoperative spine: reduction with fast spin-echo techniques. Radiology 1994; 190:565–569.
12. Tormanen J, Tervonen O, Koivula A, Junita J, Suramo I. Image technique optimization in MR imaging of a titanium alloy joint prosthesis. J Magn Reson Imaging 1996; 6:805–811.
13. Suh JS, Jeong EK, Shin KH, et al. Minimizing artifacts caused by metallic implants at MR imaging: experimental and clinical studies. AJR Am J Roentgenol 1998; 171: 1207–1213.
14. Lemmens JA, van Horn JR, den Boer J, van der Riet W, Ruijs JH. MR imaging of 22 Charnley-Muller total hip prostheses. Rofo Fortschr Rontgenstr Geb Nuklearmed 1986; 145:311–315.
15. Heindel W, Friedmann G, Bunke J, Thomas B, Firsching R, Ernestus RI. Artifacts in MR imaging after surgical intervention. J Comput Assist Tomogr 1986; 10:596–599.
16. Sprent P. Applied nonparametric statistical methods. 2nd ed. London, England: Chapman & Hall, 1993; 168–172.
17. Bakker CJG, Bhagwandien R, Moerland MA, Fuderer M. Susceptibility artifacts in 2DFT spin-echo imaging: the cylinder model revisited. Magn Reson Imaging 1993; 11:539–548.

18. Ebraheim NA, Savolaine ER, Zeiss J, Jackson WT. Titanium hip implants for improved magnetic resonance and computed tomography examinations. Clin Orthop 1992; 275:194–198.
19. Bogost GA, Lizerbram EK, Crues JV. MR imaging in evaluation of suspected hip fracture: frequency of unsuspected bone and soft-tissue injury. Radiology 1995; 197:263–267.
20. Deutsch AL, Mink JH, Wacman AD. Occult fractures of the proximal femur: MR imaging. Radiology 1989; 170:113–116.
21. Feldman F, Staron RB, Zwass A, Rubin S, Haramati N. MR imaging: its role in detecting occult fractures. Skeletal Radiol 1994; 23:439–444.
22. Autii-Poika, Joseffsson G, Konttinen Y, Lidgren L, Santavirta S, Sanzen L. Hip arthroplasty infection: current concepts. Acta Orthop Scand 1990; 61:163–169.
23. Mason MD, Zlatkin MB, Esterhai JL, Dalinka MK, Velchik MG, Kressel HY. Chronic complicated osteomyelitis of the lower extremity: evaluation with MR imaging. Radiology 1989; 173:355–359.
24. Morrison WB, Schweitzer ME, Batte WG, Radack DP, Russel KM. Osteomyelitis of the foot: relative importance of primary and secondary MR imaging signs. Radiology 1998; 207:625–632.
25. Schweitzer ME, Deely DM, Senyk R, Hume E. Not a black hole: MR imaging of the infected total knee arthroplasty. Radiology 1996; 201(P):170.
26. Cho ZH, Kim DJ, Kim YK. Total inhomogeneity correction including chemical shift and susceptibility by view angle tilting. Med Phys 1988; 15:7–11.
27. Mueller PR, Stark DD, Simeone JF, et al. MR-guided aspiration biopsy: needle design and clinical trials. Radiology 1986; 161:605–609.
28. Young IR, Cox IJ, Bryant DJ, Bydder GM. The benefits of increasing spatial resolution as a means of reducing artifacts due to field inhomogeneities. Magn Reson Med 1988; 6:585–590.
29. Haacke EM, Tkach JA, Parrish TB. Reduction of T2* dephasing in gradient field-echo imaging. Radiology 1989; 170:457–462.
30. Hilfiker P, Zanetti M, Debatin JF, McKinnon G, Holder J. Fast spin-echo inversion-recovery imaging versus fast spin-echo imaging in bone marrow abnormalities. Invest Radiol 1995; 30:110–114.
31. Camacho CR, Plewes DB, Henkelman RM. Nonsusceptibility artifacts due to metallic objects in MR imaging. J Magn Reson Imaging 1995; 5:75–88.
32. Sakurai K, Fujita N, Harada K, Kim SW, Nakanishi K, Kozuka T. Magnetic susceptibility artifact in spin-echo MR imaging of the pituitary gland. AJNR Am J Neuroradiol 1992; 13:1301–1308.
33. Bakker CJG, Bhagwandien R, Moerland MA, Ramos LMP. Simulation of susceptibility artifacts in 2D and 3D Fourier transform spin-echo and gradient-echo magnetic resonance imaging. Magn Reson Imaging 1994; 12:767–774.
34. Hennig J. Clinical applications and methodological developments of the RARE technique. Magn Reson Imaging 1988; 4:391–395.